molecules

MDPI

Article

Assessment of Various Density Functional Theory Methods for Finding Accurate Structures of Actinide Complexes

Youngjin Kwon [1], Hee-Kyung Kim [2] and Keunhong Jeong [3,*]

[1] Department of Mechanical System Engineering, Korea Military Academy, Seoul 01805, Korea; kyjchonje@kaist.ac.kr
[2] Nuclear Chemistry Research Team, Korea Atomic Energy Research Institute, Daejeon 34057, Korea; hkkim@kaeri.re.kr
[3] Department of Chemistry, Korea Military Academy, Seoul 01805, Korea
* Correspondence: doas1mind@gmail.com or doas1mind@berkeley.edu or doas1mind@kma.ac.kr; Tel.: +82-2-2197-2823

Abstract: Density functional theory (DFT) is a widely used computational method for predicting the physical and chemical properties of metals and organometals. As the number of electrons and orbitals in an atom increases, DFT calculations for actinide complexes become more demanding due to increased complexity. Moreover, reasonable levels of theory for calculating the structures of actinide complexes are not extensively studied. In this study, 38 calculations, based on various combinations, were performed on molecules containing two representative actinides to determine the optimal combination for predicting the geometries of actinide complexes. Among the 38 calculations, four optimal combinations were identified and compared with experimental data. The optimal combinations were applied to a more complicated and practical actinide compound, the uranyl complex (UO_2(2,2′-(1E,1′E)-(2,2-dimethylpropane-1,3-dyl)bis(azanylylidene)(CH_3OH)), for further confirmation. The corresponding optimal calculation combination provides a reasonable level of theory for accurately optimizing the structure of actinide complexes using DFT.

Keywords: DFT; actinides; americium (III) hexachloride; uranium hexafluoride; uranyl complex

Citation: Kwon, Y.; Kim, H.-K.; Jeong, K. Assessment of Various Density Functional Theory Methods for Finding Accurate Structures of Actinide Complexes. *Molecules* **2022**, *27*, 1500. https://doi.org/10.3390/molecules27051500

Academic Editor: Athanassios C. Tsipis

Received: 13 January 2022
Accepted: 20 February 2022
Published: 23 February 2022

1. Introduction

Density functional theory (DFT) is the most widely used method for predicting the properties of molecules. The reliability of DFT results has led to increased applications in the fields of chemistry and materials science [1–3]. DFT studies have been essential for understanding rapid reaction processes [4] and have been used to calculate the electronic structure of molecules primarily composed of organic materials or molecules containing transition metals [5,6]. For the latter, it is not possible to include a multi-reference character in a method based on a single-configuration approach to represent an almost degenerate electron state. However, recent DFT studies have overcome this problem and afforded precise results on organometallic or metal clusters [6–9]. Nevertheless, DFT-derived information on molecules consisting of 92 or more electrons, such as actinides, is lacking [10–12] due to the high radioactivity of such molecules that must be handled in safe and appropriately designed control facilities [13,14]. Furthermore, the actinide orbital interaction model is challenging to calculate owing to the emergence of spin-orbit coupling, many-electron counts, and 5f and 6d bonding orbitals [15]. DFT studies have been used as an effective way to analyze the spectrum and geometry of this interaction model [16].

DFT has been successfully employed using various functional and basis set options for the molecular modeling and analysis of actinides. In many studies on actinides, methods like B3LYP, BP86, and PBE have been used. However, combinations of these methods have not been studied [9,17–19]. Studies on organic materials and comparisons of the methodologies used for transition metals, such as Ni, Fe, La, and Gd, have

been reported. However, similar comparisons for heavy metals like actinium are insufficient [8,20,21]. Moreover, actinide materials have been studied using DFT. However, these studies do not include combinations of methods [22]. Therefore, in this study, we compared each method using relatively simple structures, americium(III) hexachloride ($AmCl_6^{3-}$) and uranium hexafluoride (UF_6), and verified that the selected methods could be used to analyze more complicated structures like the uranyl complex (UO_2(L)(MeOH), where L = (2,2′-(1E,1′E)-(2,2-dimethylpropane-1,3-dyl)bis(azanylylidene) [9,16,23,24], as shown in Figure 1. Our theory was used to describe actinide chemistry to demonstrate the reliability of the results.

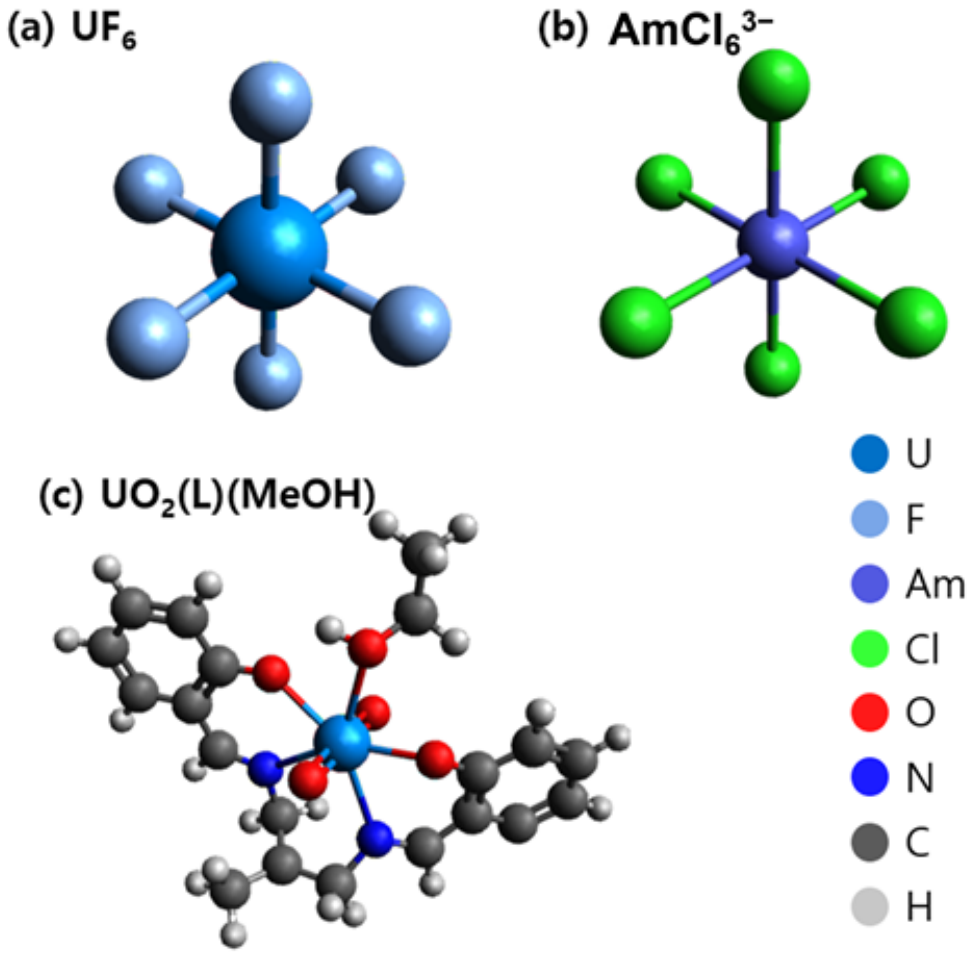

Figure 1. Molecular structure of (**a**) UF_6, (**b**) $AmCl_6^{3-}$, and (**c**) UO_2(L)(MeOH) [9,17,23,24].

2. Results and Discussion

The bond distances of UF_6 and $AmCl_6^{3-}$ were calculated using 38 different theoretical combinations and are shown in Figures 2 and 3, respectively. The complex molecular structure of UO_2(L)(MeOH) was calculated based on the three most accurate calculation methods used to calculate the structures of $AmCl_6^{3-}$ and UF_6. The calculation methods used in this study optimized the geometries of atoms in the molecule and predicted the structure closest to that obtained from the experimental results. We represent the mean absolute deviation (MAD) between the experimental and calculated values instead of plotting the length of all calculated bonds.

2.1. Uranium Hexafluoride

UF_6 is a widely known molecular compound used as a key ingredient in the enrichment of natural uranium [23]. Studies have been conducted based on the mean distance determined from automatic neutron diffractometry, infrared and Raman spectra, electron

diffraction, and quantum calculations [18,21,24,25]. The mean bond lengths of the molecular structures optimized using 38 DFT calculation combinations are shown in Figure 2. The MAD calculations showed deviations ranging between 0.0001 Å and 0.04 Å. (see Supplementary Materials Table S1).

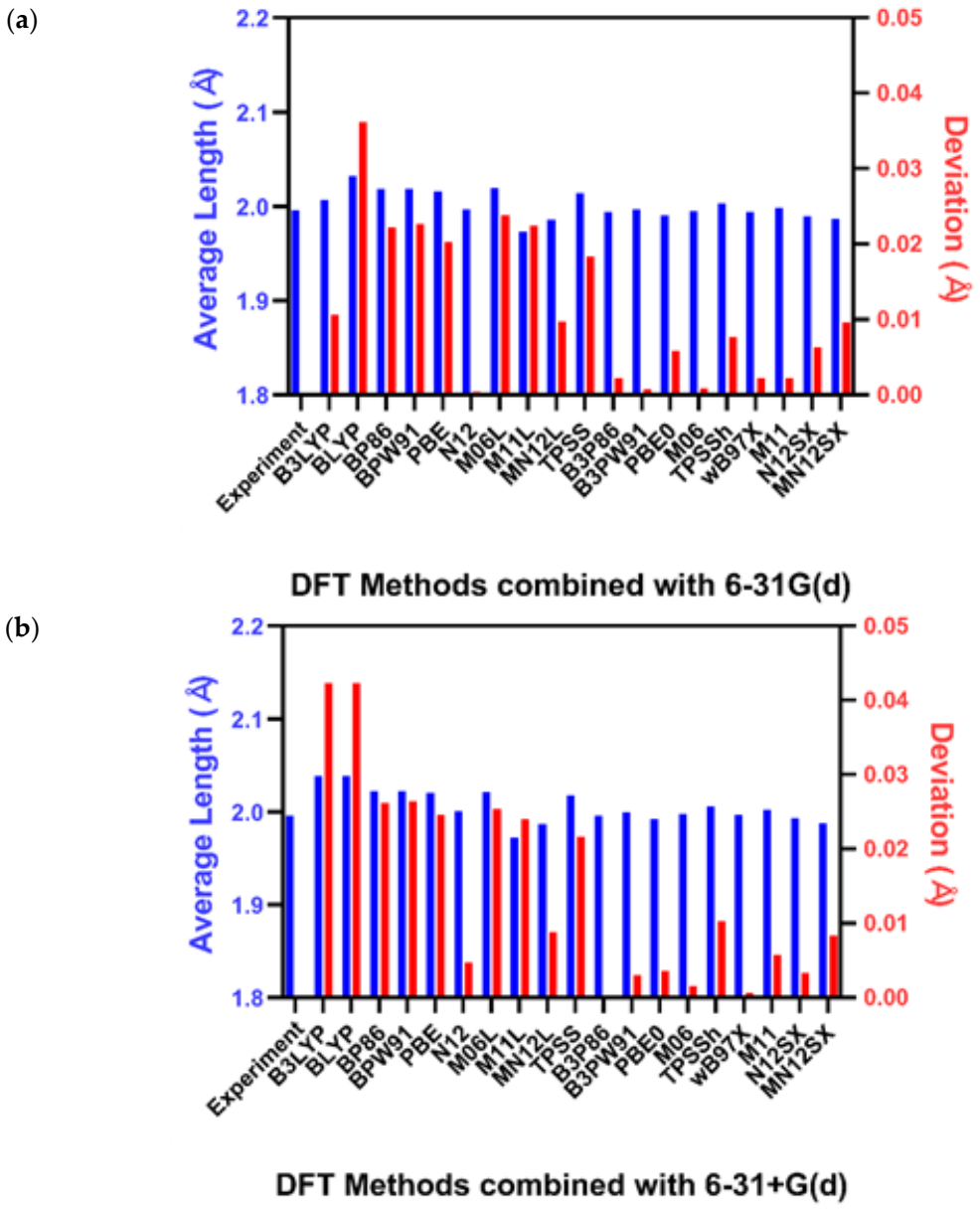

Figure 2. Average length of U-F bonds in the optimized structure with (**a**) 6-31G(d) and (**b**) 6-31+G(d) [23].

2.2. Americium (III) Hexachloride

The structure of hexahedral $AmCl_6^{3-}$ was studied using DFT calculations and single-crystal X-ray diffraction (SCXD) [9]. The optimal distances were calculated using the combinations of DFT calculations used for UF_6. A comparative analysis with reported experimental values is shown in Figure 3. PBE0/6-31G(d) and PBE0/6-31+G(d) were omitted because they did not converge despite extended time with an additional grid and a maximum cycle for the XQC algorithm. The MAD of the average bond length was between 0.06 Å and 0.15 Å.

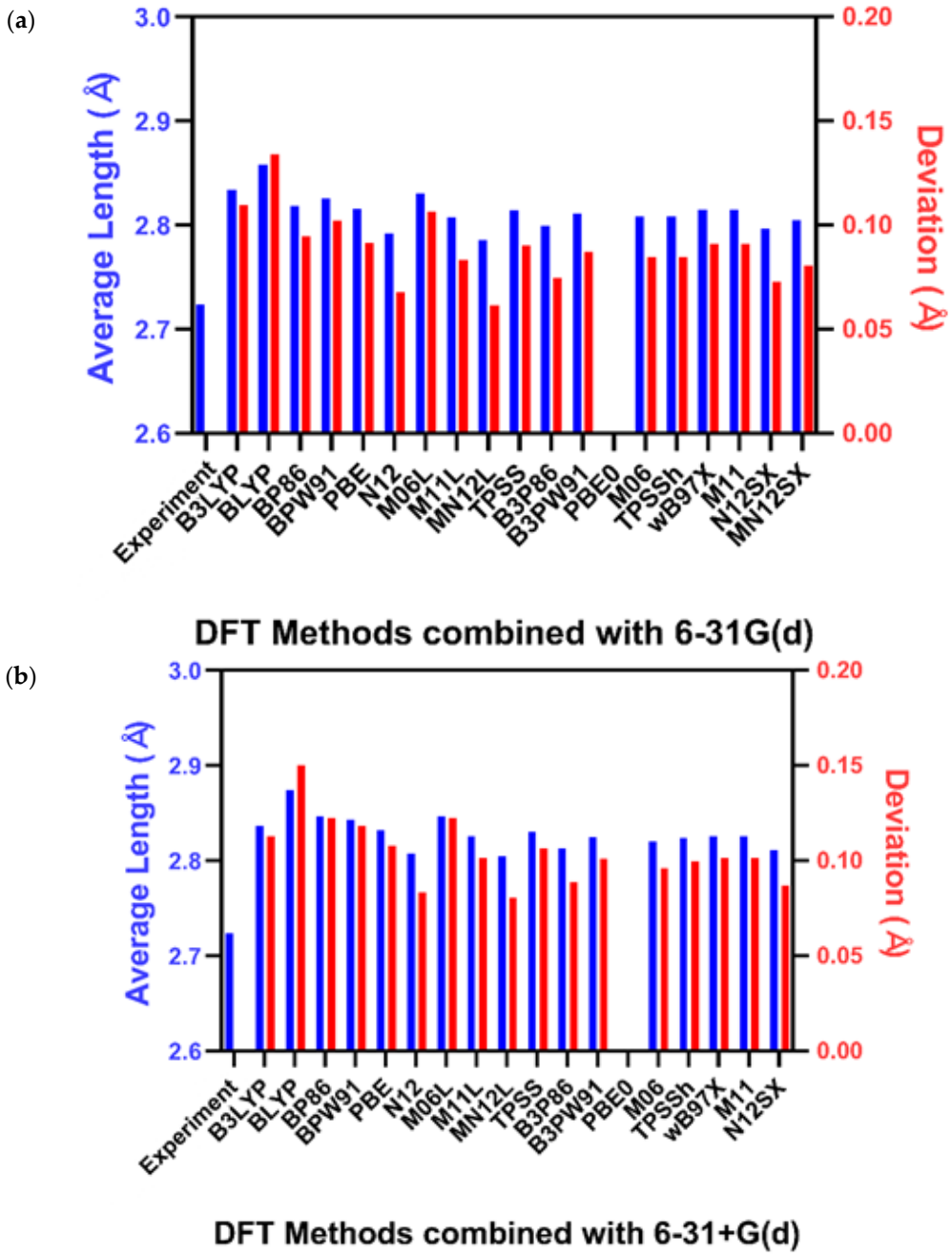

Figure 3. Average bond length of Am-Cl bonds in the optimized structure with (**a**) 6-31G(d) and (**b**) 6-31+G(d) [9].

2.3. Uranyl Complex (UO_2(L)(MeOH))

Despite the structural deviation between UF_6 and $AmCl_6^{3-}$ due to the charge difference and different configurations of valence electrons, which results in different bonding properties, the most accurate structures were the same: N12/6-31G(d), B3P86/6-31G(d), M06/6-31G(d), and B3PW91/6-31G(d). The additional diffuse function did not provide a more accurate optimized structure for $AmCl_6^{3-}$ or UF_6. Despite the contentious relationship between covalency in f-element systems and structures, both octahedral structures play the same role in the bonding model [26]. Therefore, the increased covalent bonding characteristics play a major role in the interaction. For future applications, the analysis was conducted on a uranyl complex (UO_2(L)(MeOH)) to verify the accuracy of three of the four optimized calculations (B3P86/6-31G(d), M06/6-31G(d), and B3PW91/6-31G(d))

when applied to larger, more complicated molecular structures [17]. N12/6-31G(d) was omitted because it could not be optimized despite our best efforts. The MAD of the lengths and angles between molecules was measured, and the results were compared, as shown in Figure 4 and Table 1. The results obtained by all these methods agreed with experimental data within 0.05 Å in length and 1.5° in bonding angle, with small deviations between methods, confirming that our systemic method for finding the optimal level of theory for calculating the structure of actinide complexes works well. B3PW91/6-31G(d) exhibited the smallest MAD among the three calculation combinations and accurately predicted the structure, in line with the experimental data, with length and angle deviations of less than 0.04 Å and 1.4°, respectively. Individual bond length and bond angle comparisons between each calculated result and the experimental result were carried out, showing that B3PW91 was the most accurate method for the experimental structure.

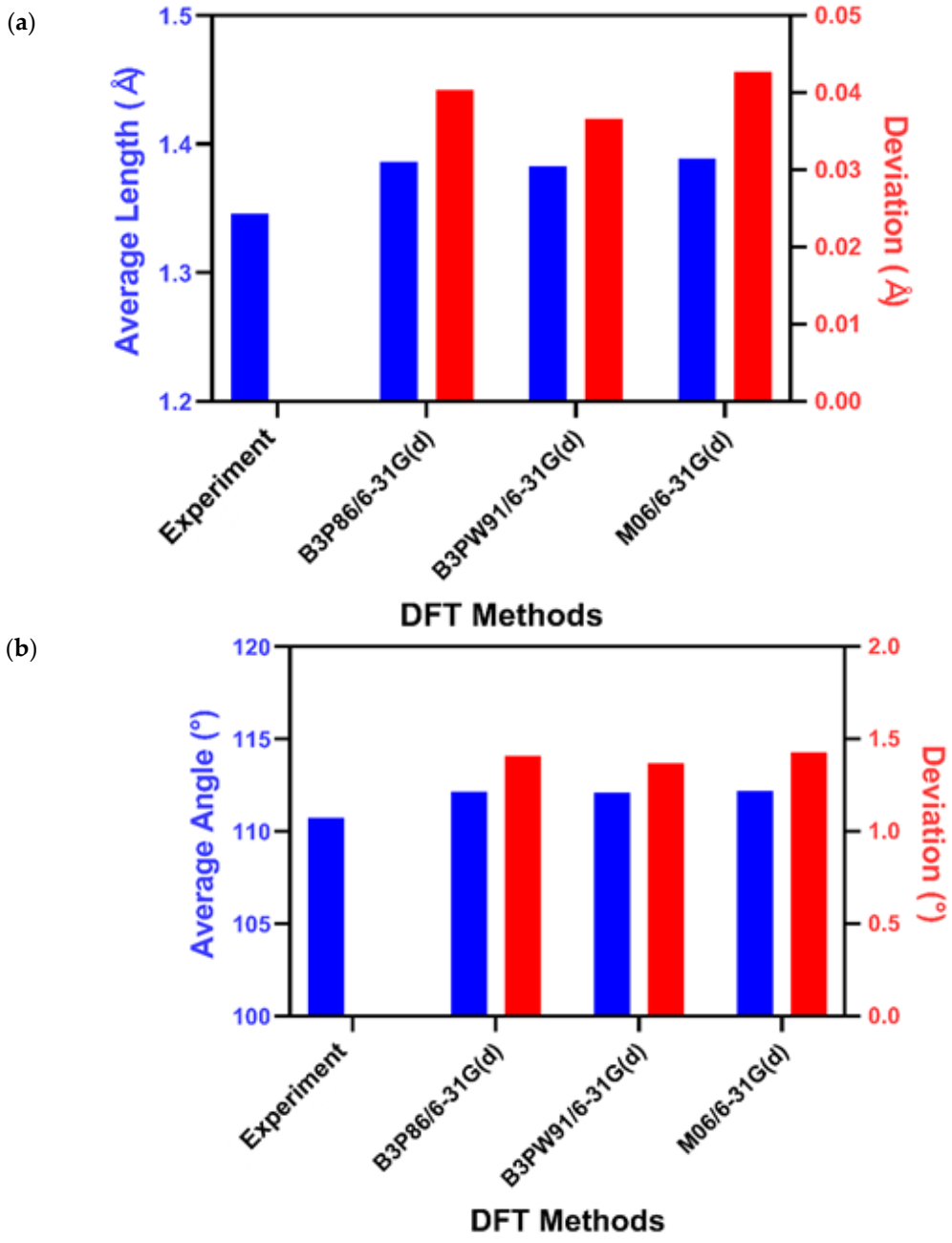

Figure 4. (**a**) Average bond length and (**b**) average angle of UO_2(L)(MeOH) in the optimized structure [17].

Table 1. Average bond length and average angle of UO_2(L)(MeOH) in the optimized structure.

DFT Method Combination		Average Length (Å)	Deviation (Å)	Average Angle (°)	Deviation (°)
Experiment [17]		1.34601	-	110.7458	-
6-31G(d)	B3P86	1.386322	0.040312	112.1528	1.407
	B3PW91	1.382651	0.036641	112.1132	1.3674
	M06	1.388692	0.042682	112.1715	1.4257

3. Computational Methods

All calculations were performed using the Gaussian09 software package [27]. $AmCl_6^{3-}$ and UF_6 were optimized with frequency calculations using 19 functionals with two basis sets, resulting in 38 possible combinations of the levels of theory. After examining each frequency without an imaginary number, the average length of each bond was compared to the experimental molecular length reported in the literature [9,23]. We selected DFT calculations based on recent theoretical studies on actinide chemistry: B3LYP, BLYP, BP86, BPW91, PBE, N12, M06L, M11L, MN12L, TPSS, B3P86, B3PW91, PBE0, M06, TPSSh, wB97X, M11, N12SX, MN12SX, and the basis set for H, O, C, N, F, and Cl with 6-31G(d) to obtain relatively light complexity and accurate theoretical results [28–31]. Ligands with anions bind loosely on the actinides, and diffuse function addition may be better for precise descriptions of the actinide ligands' complex structures. Therefore, 6-31+G(d) was used for theoretical calculations [8,21,32,33]. The ECP60MWB relativistic effective core potential and the associated basis set developed by the Stuttgart–Cologne group were selected to describe americium and uranium [29]. Several combinations of calculations were applied to UO_2(L)(MeOH), and the results were compared to prove its accuracy [17]. The developed DFT method is one of the most accurate ones for computing the electronic structure of solids [34–37] and will help study actinide materials.

4. Conclusions

The properties of actinide complexes are difficult to optimize using DFT due to unreliable theoretical methods for compounds containing more than 92 electrons. Therefore, a systematic study of methods for obtaining the theoretical structures of actinide complexes is significant for future research on actinide chemistry. This study does not contain the full relativistic effect in actinides. However, a scalar-relativistic effect is considered that can be applied to future studies. Here, two representative structures of actinide complexes, UF_6 and $AmCl_6^{3-}$, were used to determine the best DFT functions. From 38 computational combinations, the optimal combinations were evaluated by optimizing the geometries of the molecules and comparing the calculated results with the experimental values. The four most promising levels of theory for the two actinides were obtained and applied to UO_2(L)(MeOH) to confirm the accuracy of the optimal computational methods when applied to large and complex molecular structures. Finally, the B3PW91/6-31G(d) calculation yielded structures closest to the predicted actinide structures, providing a standard for establishing the level of theory of actinide complexes in the future.

Supplementary Materials: Supplementary materials are available online. Table S1: Average bond length of U-F bonds in the optimized structure with 6-31G(d) and with 6-31+G(d) [23]; Table S2: Average bond length of Am-Cl bonds in the optimized structure with 6-31G(d) and with 6-31+G(d) [9]. Table S3: (a) Bond length and (b) Angle of UO2(L)Alc. in the optimized structure [17].

Author Contributions: Y.K.: Resources, writing (original draft, review, and editing), investigation, data curation, formal analysis, software, validation, and visualization. H.-K.K.: Validation and writing (review and editing). K.J.: Conceptualization, supervision, writing (review and editing), project administration, methodology, and software. All authors have read and agreed to the published version of the manuscript.

Funding: This work was supported by a National Research Foundation of Korea (NRF) grant funded by the Korean government (MSIT) (No. 2020R1C1C1007888).

Data Availability Statement: Data is contained within the article or Supplementary Materials.

Acknowledgments: The authors thank anonymous reviewer for providing constructive feedback to improve the manuscript.

Conflicts of Interest: The authors declare no conflict of interest.

Sample Availability: Samples of the compounds are not available from the authors.

References

1. Jones, R.O. Density functional theory: Its origins, rise to prominence, and future. *Rev. Mod. Phys.* **2015**, *87*, 897–923. [CrossRef]
2. Janesko, B.G. Replacing hybrid density functional theory: Motivation and recent advances. *Chem. Soc. Rev.* **2021**, *50*, 8470–8495. [CrossRef] [PubMed]
3. El-Nahas, A.M.; Simmie, J.; Mangood, A.H.; Hirao, K.; Song, J.-W.; Watson, M.A.; Taketsugu, T.; Koga, N. Assessment of hybrid, meta-hybrid-GGA, and long-range corrected density functionals for the estimation of enthalpies of formation, barrier heights, and ionisation potentials of selected C1–C5 oxygenates. *Mol. Phys.* **2015**, *113*, 1630–1635. [CrossRef]
4. Harper, L.K.; Shoaf, A.L.; Bayse, C.A. Predicting trigger bonds in explosive materials through Wiberg bond index analysis. *Phys. Chem. Chem. Phys.* **2015**, *16*, 3886–3892. [CrossRef]
5. Jeong, K.; Sung, I.; Joo, H.U.; Kwon, T.; Yuk, J.M.; Kwon, Y.; Kim, H. Molecular design of nitro-oxide-substituted cycloalkane derivatives for high-energy-density materials. *J. Mol. Struct.* **2020**, *1212*, 128128. [CrossRef]
6. Chaves, A.S.; Piotrowski, M.J.; Da Silva, J.L.F. Evolution of the structural, energetic, and electronic properties of the 3d, 4d, and 5d transition-metal clusters (30 TMn systems for n = 2–15): A density functional theory investigation. *Phys. Chem. Chem. Phys.* **2017**, *19*, 15484–15502. [CrossRef]
7. O'Connor, N.J.; Jonayat, A.S.M.; Janik, M.J.; Senftle, T.P. Interaction trends between single metal atoms and oxide supports identified with density functional theory and statistical learning. *Nat. Catal.* **2018**, *1*, 531–539. [CrossRef]
8. Narendrapurapu, B.S.; Richardson, N.A.; Copan, A.V.; Estep, M.L.; Yang, Z.; Schaefer, I.H.F. Investigating the effects of basis set on metal–metal and metal–ligand bond distances in stable transition metal carbonyls: Performance of correlation consistent basis sets with 35 density functionals. *J. Chem. Theory Comput.* **2013**, *9*, 2930–2938. [CrossRef]
9. Cross, J.N.; Su, J.; Batista, E.R.; Cary, S.K.; Evans, W.J.; Kozimor, S.A.; Mocko, V.; Scott, B.L.; Stein, B.W.; Windorff, C.J.; et al. Covalency in americium(III) hexachloride. *J. Am. Chem. Soc.* **2017**, *139*, 8667–8677. [CrossRef]
10. Polinski, M.J.; Garner, E.B.; Maurice, R.; Planas, N.; Stritzinger, J.T.; Parker, T.G.; Cross, J.; Green, T.D.; Alekseev, E.; Van Cleve, S.M.; et al. Unusual structure, bonding and properties in a californium borate. *Nat. Chem.* **2014**, *6*, 387–392. [CrossRef]
11. Kullie, O. Tunneling time in attosecond experiments, intrinsic-type of time. Keldysh, and Mandelstam–Tamm time. *J. Phys. B At. Mol. Opt. Phys.* **2016**, *49*, 095601. [CrossRef]
12. Silver, M.A.; Cary, S.K.; Johnson, J.A.; Baumbach, R.E.; Arico, A.A.; Luckey, M.; Urban, M.; Wang, J.C.; Polinski, M.J.; Chemey, A.; et al. Characterization of berkelium(III) dipicolinate and borate compounds in solution and the solid state. *Science* **2016**, *353*, aaf3762. [CrossRef] [PubMed]
13. Iasir, A.R.M.; Hammond, K.D. Pseudopotential for plane-wave density functional theory studies of metallic uranium. *Comput. Mater. Sci.* **2019**, *171*, 109221. [CrossRef]
14. Natrajan, L.S.; Swinburne, A.N.; Andrews, M.B.; Randall, S.; Heath, S.L. Redox and environmentally relevant aspects of actinide(IV) coordination chemistry. *Coord. Chem. Rev.* **2014**, *266–267*, 171–193. [CrossRef]
15. Gendron, F.; Autschbach, J. Ligand NMR chemical shift calculations for paramagnetic metal complexes: 5f1 vs 5f2 Actinides. *J. Chem. Theory Comput.* **2016**, *12*, 5309–5321. [CrossRef] [PubMed]
16. Su, J.; Batista, E.R.; Boland, K.S.; Bone, S.E.; Bradley, J.A.; Cary, S.K.; Clark, D.L.; Conradson, S.D.; Ditter, A.S.; Kaltsoyannis, N.; et al. Energy-Degeneracy-Driven Covalency in Actinide Bonding. *J. Am. Chem. Soc.* **2018**, *140*, 17977–17984. [CrossRef]
17. Azam, M.; Velmurugan, G.; Wabaidur, S.M.; Trzesowska-Kruszynska, A.; Kruszynski, R.; Al-Resayes, S.I.; Alothman, Z.; Venuvanalingam, P. Structural elucidation and physicochemical properties of mononuclear Uranyl(VI) complexes incorporating dianionic units. *Sci. Rep.* **2016**, *6*, 32898. [CrossRef]
18. Choi, Y.J.; Lee, Y.S. Spin–orbit density functional theory calculations for heavy metal monohydrides. *J. Chem. Phys.* **2003**, *119*, 2014. [CrossRef]
19. Belkhiri, L.; Le Guennic, B.; Boucekkine, A. DFT Investigations of the Magnetic Properties of Actinide Complexes. *Magnetochemistry* **2019**, *5*, 15. [CrossRef]
20. Vetere, V.; Adamo, C.; Maldivi, P. Performance of the 'parameter free' PBE0 functional for the modeling of molecular properties of heavy metals. *Chem. Phys. Lett.* **2000**, *325*, 99–105. [CrossRef]
21. Rassolov, V.A.; Ratner, M.A.; Pople, J.A.; Redfern, P.C.; Curtiss, L.A. 6-31G* basis set for third-row atoms. *J. Comput. Chem.* **2001**, *22*, 976–984. [CrossRef]
22. Schreckenbach, G.; Hay, P.J.; Martin, R.L. Density functional calculations on actinide compounds: Survey of recent progress and application to [UO2X4]2-(X=F, Cl, OH) and AnF6 (An=U, Np, Pu). *J. Comp. Chem.* **1999**, *20*, 70–90. [CrossRef]
23. Weinstock, B.; Goodman, G.L. Vibrational properties of hexafluoride molecules. *Adv. Chem. Phys.* **1965**, *9*, 169. [CrossRef]

24. Levy, J.H.; Taylor, J.C.; Wilson, P.W. Structure of fluorides. Part XII. Single-crystal neutron diffraction study of uranium hexafluoride at 293 K. *J. Chem. Soc. Dalton Trans.* **1976**, 219–224. [CrossRef]
25. Kimura, M.; Schomaker, V.; Smith, D.W.; Weinstock, B. Electron-diffraction investigation of the hexafluorides of tungsten, osmium, iridium, uranium, neptunium, and plutonium. *J. Chem. Phys.* **1968**, *48*, 4001. [CrossRef]
26. Lu, E.; Sajjad, S.; Berryman, V.E.J.; Wooles, A.J.; Kaltsoyannis, N.; Liddle, S.T. Emergence of the structure-directing role of f-orbital overlap-driven covalency. *Nat. Commun.* **2019**, *10*, 1–10. [CrossRef]
27. Frisch, M.; Trucks, G.; Schlegel, H.B.; Scuseria, G.E.; Robb, M.A.; Cheeseman, J.R.; Scalmani, G.; Barone, V.; Mennucci, B.; Petersson, G. *Gaussian 09*; Revision d. 01; Gaussian, Inc.: Wallingford, CT, USA, 2009; Volume 201, Available online: http://www.gaussian.com/ (accessed on 10 February 2022).
28. Jeong, K.; Woo, S.M.; Bae, S. DFT study on the bonding properties of Pu(III) and Pu(IV) chloro complexes. *J. Nucl. Sci. Technol.* **2018**, *55*, 424–428. [CrossRef]
29. Jeong, K.; Jeong, H.J.; Woo, S.M.; Bae, S. Prediction of binding stability of Pu(IV) and PuO2(VI) by nitrogen tridentate ligands in aqueous solution. *Int. J. Mol. Sci.* **2020**, *21*, 2791. [CrossRef]
30. Jeong, K.; Woo, S.M.; Park, J.; Bae, S. Detection of hydrolyzed plutonium chloride compounds generated by moisture intrusion of pyroprocessing hot cell using density functional theory. *J. Radioanal. Nucl. Chem. Artic.* **2020**, *325*, 101–110. [CrossRef]
31. Kim, H.-K.; Jeong, K.; Cho, H.-R.; Kwak, K.; Jung, E.C.; Cha, W. Study of aqueous Am(III)-aliphatic dicarboxylate complexes: Coordination mode-dependent optical property and stability changes. *Inorg. Chem.* **2020**, *59*, 13912–13922. [CrossRef]
32. Zhao, Y.; Truhlar, D.G. The M06 suite of density functionals for main group thermochemistry, thermochemical kinetics, noncovalent interactions, excited states, and transition elements: Two new functionals and systematic testing of four M06-class functionals and 12 other functionals. *Theor. Chem. Acc.* **2008**, *120*, 215–241. [CrossRef]
33. Perdew, J.P.; Chevary, J.A.; Vosko, S.H.; Jackson, K.A.; Pederson, M.R.; Singh, D.J.; Fiolhais, C. Atoms, molecules, solids, and surfaces: Applications of the generalized gradient approximation for exchange and correlation. *Phys. Rev. B* **1992**, *46*, 6671–6687, Erratum: *Phys. Rev. B* **1993**, *48*, 4978. [CrossRef] [PubMed]
34. Merabet, B.; Almaliky, A.J.; Reshak, A.; Ramli, M.M.; Bila, J. Dielectric absorption correlated to ferromagnetic behavior in (Cr, Ni)-codoped 4H–SiC for microwave applications. *J. Mol. Struct.* **2022**, *1248*, 131462. [CrossRef]
35. Tabassam, S.; Reshak, A.H.; Murtaza, G.; Muhammad, S.; Laref, A.; Yousaf, M.; Al Bakri, A.M.; Bila, J. Co2YZ (Y= Cr, Nb, Ta, V and Z= Al, Ga) Heusler alloys under the effect of pressure and strain. *J. Mol. Graph. Model.* **2021**, *104*, 107841. [CrossRef]
36. Hoat, D.M.; Amirian, S.; Alborznia, H.; Laref, A.; Reshak, A.H.; Naseri, M. Strain effect on the electronic and optical properties of 2D Tetrahexcarbon: A DFT-based study. *Indian J. Phys.* **2021**, *95*, 2365–2373. [CrossRef]
37. Husain, M.; Rahman, N.; Reshak, A.H.; Zulfiqar; Habib, A.; Ali, S.; Laref, A.; Al Bakri, A.M.M.; Bila, J. Insight into the physical properties of the inter-metallic titanium-based binary compounds. *Eur. Phys. J. Plus* **2021**, *136*, 1–10. [CrossRef]